Supplementary information for "Contribution of Coiled-coil Assembly to Ca^{2+}/Calmodulin-dependent Inactivation of TRPC6 Channel and its Impacts on FSGS-associated Phenotypes"

Table of contents

SI methods

Simultaneous detection of TRPC currents and intracellular Ca^{2+}.

TRPC6/M_1R co-transfected HEK293 cells were seeded on coverslips, and incubated for 45 min in 5 μM Fura-4/AM. The cells were then washed with external solution and mounted on a Nikon TE3000 Eclipse microscope (× 60, 0.9 NA objective) and visualized by a CCD camera (Evolve 512, Roper Scientific). The cells were alternatively excited with 340/380 nm wavelengths and the emission was recorded at 512 nm. Cells which had Fura-4 and GFP dual expression were selected, and patch-clamped using whole-cell configuration (V_h = -50 mV) with the lower Ca^{2+} buffering condition (see Methods). Images were digitized as 512×512 pixels by 16 bit arrays. Fluorescence ratios between 340 nm and 380 nm which are correlated with $[Ca^{2+}]_i$ were obtained by averaging intensities from regions of interest (ROIs) and analyzed by a custom written program in MATLAB (Mathworks).[1]

Simultaneous detection of TRPC currents and $PI(4,5)P_2$.

Detailed methods are described in a previous report.[2] Briefly, HEK293 cells on coverslips were co-transfected with equal amounts of TRPC6 channels, and $PI(4,5)P_2$ sensor proteins: YFP- pleckstrin-homology domain (PHd) and CFP-PHd, with or without M_1R, and placed in a perfusion chamber. Images were digitized as 512 × 512 pixels by 16-bit arrays. For sampling, the illumination shutter in the lamp house was opened for 100 ms every 300 ms. Averaged intensities from ROIs (typically 10×10 to 25×25 square pixels) that include the cell membrane and cytosol were used for FRET calculations. For modeling and fitting statistics, $PI(4,5)P_2$ hydrolysis pathway by PLC were formulated as ordinary differential equations, and the

concentrations of $PI(4,5)P_2$ and DAG derived from these were incorporated into the channel-operation models. Simulations were performed in Excel (Microsoft) using the forward Euler method with a time step of 0.05 s. Individual steps were translated into differential equations based on the proposed kinetic scheme. Fitting the models to the experimental data of TRPC6 currents at the low Ca^{2+} buffering condition was performed by a generalized reduced gradient algorithm of the solver function in Excel.

Preparation for ^{13}C, ^{15}N-doubly labeled CBDp.

Preparation of the labeled TRPC6 (CBDp, 853−874 a.a.) is as follows. 10xHis-SUMO fusion CBD was expressed in *E. coli* BL-21 (DE3) (Novagen). This was cultured with M9 Minimal Medium including ^{13}C labeled glucose and ^{15}N labeled ammonium chloride upon induction by 0.2 mM IPTG for 18 hours at OD_{600} = 1.0. Cell pellets were initially resuspended in lysis buffer containing 20 mM Tris-HCl (pH 8.0), 300 mM NaCl, 1mM DTT and cOmplete EDTA free protease inhibitor cocktail tablet (Roche). Resuspended pellets were crushed for 10 min with a sonicator (Qsonica). Cell debris were collected following centrifugation at 15,000 rpm for 30 min in 4 °C. Collected debris were vigorously washed in the buffer containing 20 mM Tris-HCl (pH 8.0), 300 mM NaCl and 1% Triton-X100. Washed debris were resuspended in denaturation buffer containing 20 mM Tris-HCl (pH 8.0), 300 mM NaCl and 6 M GdnHCl. Denatured debris were removed following centrifugation at 15,000 rpm for 30 min in 4 °C and filtration with 0.45 μm filter (Millipore). Filtered denatured sample were added to Ni-NTA resin Purification Column (10 ml) (Roche) pre-equilibrated with 4 column volume (CV) denaturation buffer and stirred for 1 hour in 4 °C. Column washing was conducted using 10 CV denaturation buffer. 10xHis-SUMO3 tag fusion CBD was eluted with 6 CV elution buffer

containing 20 mM Tris-HCl (pH 8.0), 300 mM NaCl, 6 M GdnHCl and 400 mM Imd-HCl. Eluted fractions were concentrated with Amicon Ultra-15 3,000 nominal molecular weight limit (NMWL) (Millipore) to 2 ml and, for refolding, rapidly diluted to 10 times volume in refolding buffer containing 20 mM Tris-HCl (pH 8.0), 300 mM NaCl, 400 mM Arg-HCl and 20 mM DTT. The tag sequence of the refolded 10xHis-SUMO3 tag fusion CBD was eliminated by SENP2. Tag eliminated CBDp was concentrated and buffer was exchanged to lysis buffer with Amicon Ultra-15 3,000 NMWL. Concentrated CBDp was acidified with 1% TFA down to pH smaller than 2.0 and was injected to Presep-C C18 (Wako, Japan) column pre-equilibrated with 5% acetonitrile. Column washing was conducted using 10 CV 5% acetonitrile and CBDp was eluted by 10 CV 30% acetonitrile. Solvent of eluted fractions were removed with evaporator and freeze dryer (EYELA). Dried sample was resuspended in 1% TFA and injected to ODS-A column (YMC). Fractions of CBDp were eluted by 80% acetonitrile gradient. Solvent of eluted fractions were removed with evaporator and freeze dryer. CBDp purity was analyzed in 15% SDS-PAGE and this ^{13}C, ^{15}N-labeled CBDp powder was kept in -80 °C.

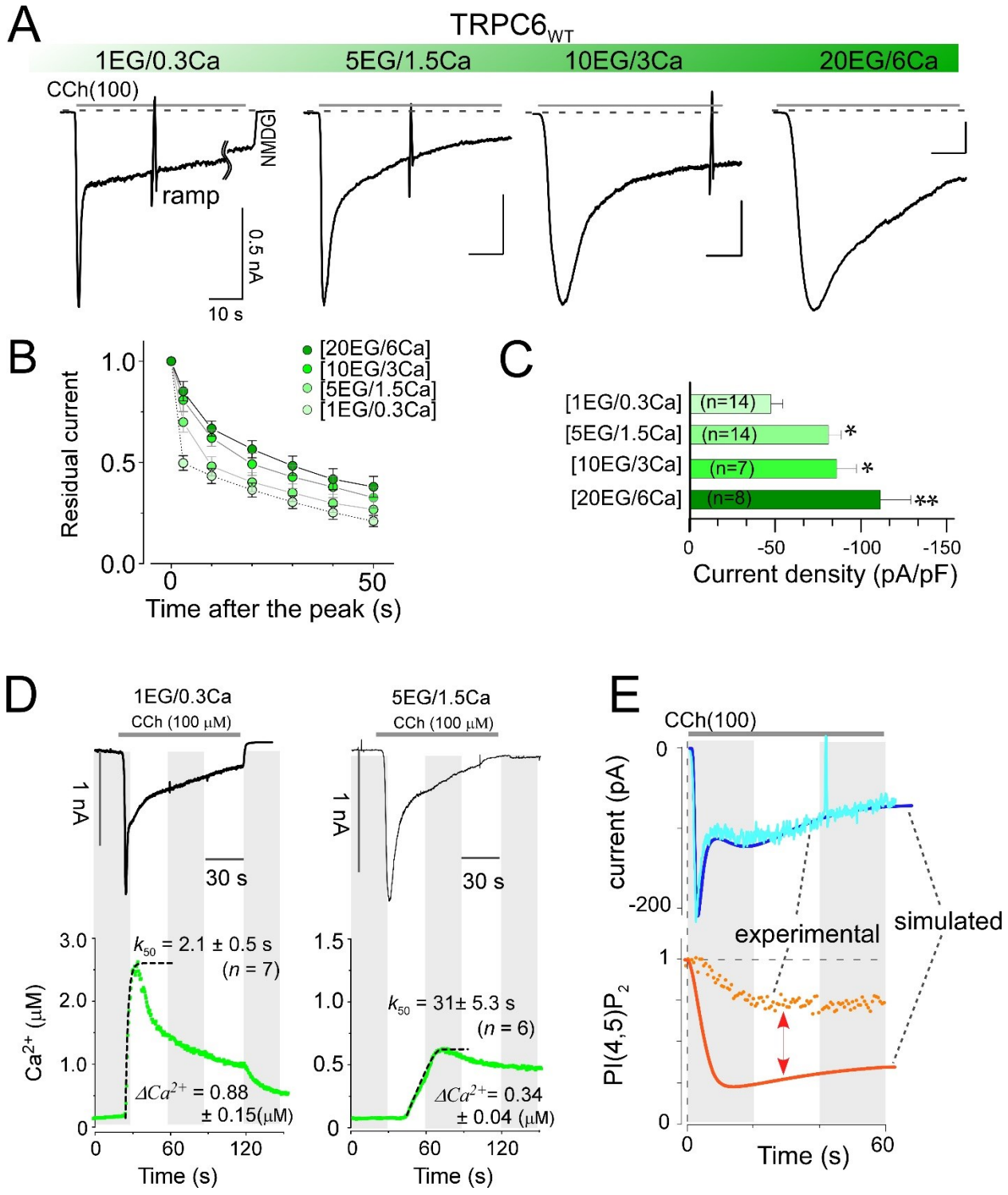

Figure S1. Ca^{2+} buffering effects on TRPC6 current. (*A*) Inward TRPC6 currents evoked by 100 μM CCh, shown as gray bar on top, with holding potential at -50 mV. Sharp noises indicate a

ramp pulse (1 s) from -100 mV to +100 mV to confirm a typical doubly rectifying *I-V* curve of TRPC6 currents.[3] An NMDG-based solution was applied to check for leak currents. Effects of Ca^{2+} buffering in patch-pipette solution can be observed from left to right in increasing buffering capacity. Vertical and horizontal bars were kept constant at 500 pA and 10 s, here and throughout. (*B*) To quantify the extent of the inactivation, the time course of current decay was normalized to the initial peak. The fraction of current remaining after the peak was plotted from 0 to 50 s. Solid spheres filled with light to dark green color are dependent on the pipette Ca^{2+} buffering capacity (lightest green: 1EGTA/0.3$CaCl_2$, dark green: 20EGTA/6$CaCl_2$). The data are presented as the means ± SEM. (*C*) Peak current densities (pA/pF) from various Ca^{2+} buffering conditions. The peak almost always appeared within a few seconds after the CCh stimulation. Higher Ca^{2+} buffering conditions are compared to 1EG/0.3Ca. (*D*) Simultaneous measurement of TRPC6 currents and $[Ca^{2+}]_i$. TRPC6 currents were recorded by whole-cell configuration at Ca^{2+} bufferings [1EG/0.3Ca] (left) and [5EG/1.5Ca] (right). Measured $[Ca^{2+}]_i$ were shown in the lower panels. The [5EG/1.5Ca] condition was well-buffered for both $\Delta[Ca^{2+}]_i$ and its kinetics. k_{50} indicates the measured time required for 50% increase to reach the maximum $[Ca^{2+}]_i$. (*E*) Receptor-activated $PI(4,5)P_2$ levels were monitored by the FRET-based $PI(4,5)P_2$ sensor; simultaneously with TRPC6 current. The experimental currents and $PI(4,5)P_2$ are shown as light blue line and orange dots, respectively. The simulated TRPC6 current and $PI(4,5)P_2$ with *SPD* model[2] are represented by solid blue and orange lines, respectively. The simulated $PI(4,5)P_2$ (solid orange line) is severely depleted and thus fully incompatible with the actual $PI(4,5)P_2$ reduction (orange circles).

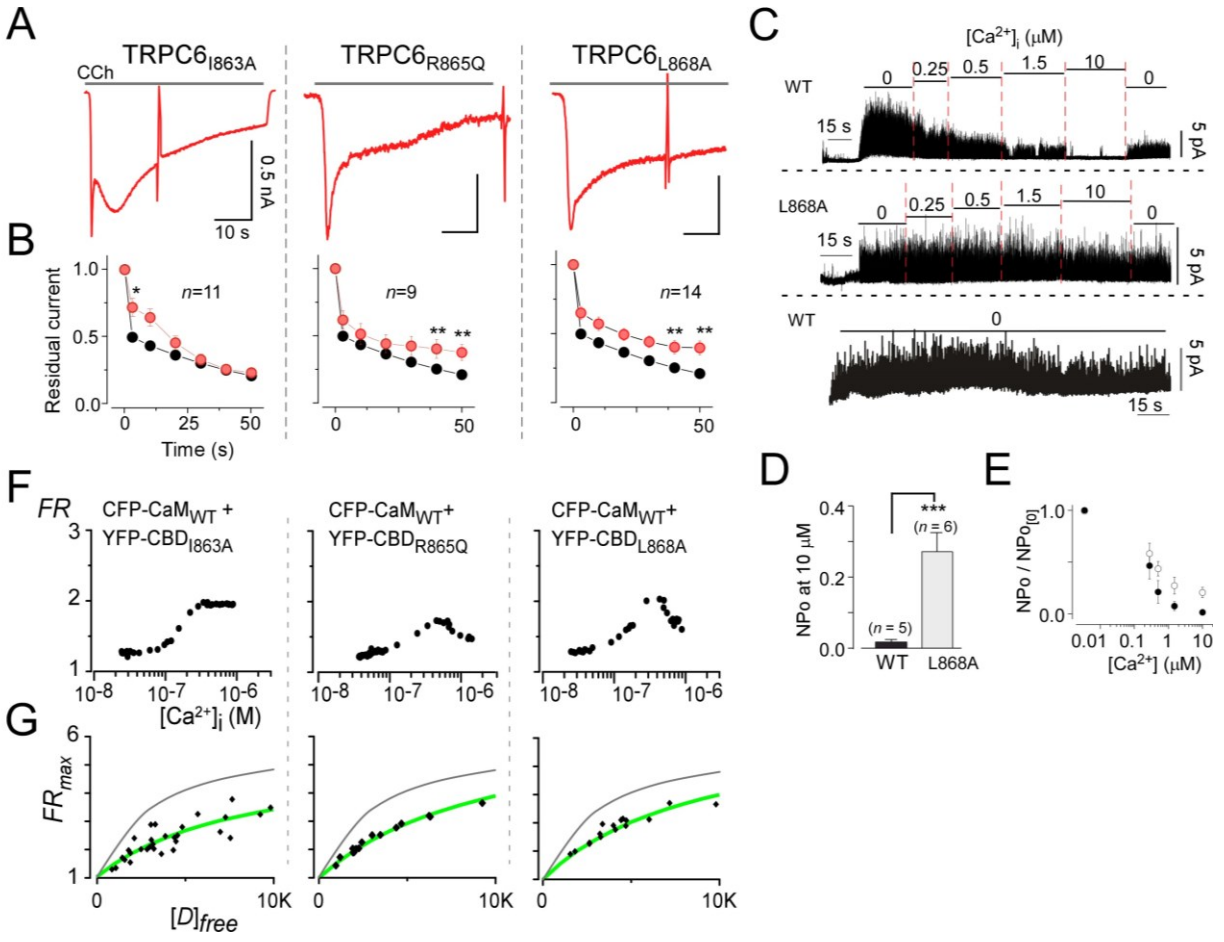

Figure S2. Functional and biophysical analyses of CBD mutants. (*A*) Whole-cell current traces for CBD mutants ($TRPC6_{I863A}$, $TRPC6_{R865Q}$, $TRPC6_{L868A}$). (*B*) Residual currents of CBD mutants after the peak shown in red circles. Black circles indicate control data from TRPC6 only (n = 14, CaM_{endo}), here and throughout. The data were presented as the means ± SEM. (*C*) Inside-out recording from $TRPC6_{WT}$ (top) and $TRPC6_{L868A}$ mutants (middle). Sequential increase in the $[Ca^{2+}]_i$ represented by a black overhead bar. Bottom panel represents control recording for $TRPC6_{WT}$ wherein $[Ca^{2+}]_i$ was held at zero and no clear desensitization was observed. (*D*) The open channel probability (NPo) at the highest $[Ca^{2+}]_i$ (10 μM Ca^{2+}) is shown in the bar graphs. The *P*-values were calculated using one-way ANOVA. (*E*) TRPC6 (black

circles) and TRPC6$_{L868A}$ (open circles) are represented as a plot of normalized NPo versus $[Ca^{2+}]_i$. Normalized NPo values were obtained by dividing actual NPo values with NPo at zero $[Ca^{2+}]_i$. (*F*) Representative Ca^{2+}-dependent binding of CBD mutants with CaM. (*G*) Quantification of affinity of binding of CBD mutants to CaM by plotting donor free concentrations $[D]_{free}$ against FRET signal (*FR*). Data from various cells were collected at maximum *FR* values, shown in Figure S2, *F*. The grey line represents control CaM_{WT} versus CBD_{WT} taken from Figure 1D. Green lines represent fitting of respective CBD_{MUT} versus CaM_{WT}. Numerical values are shown in Table S1.

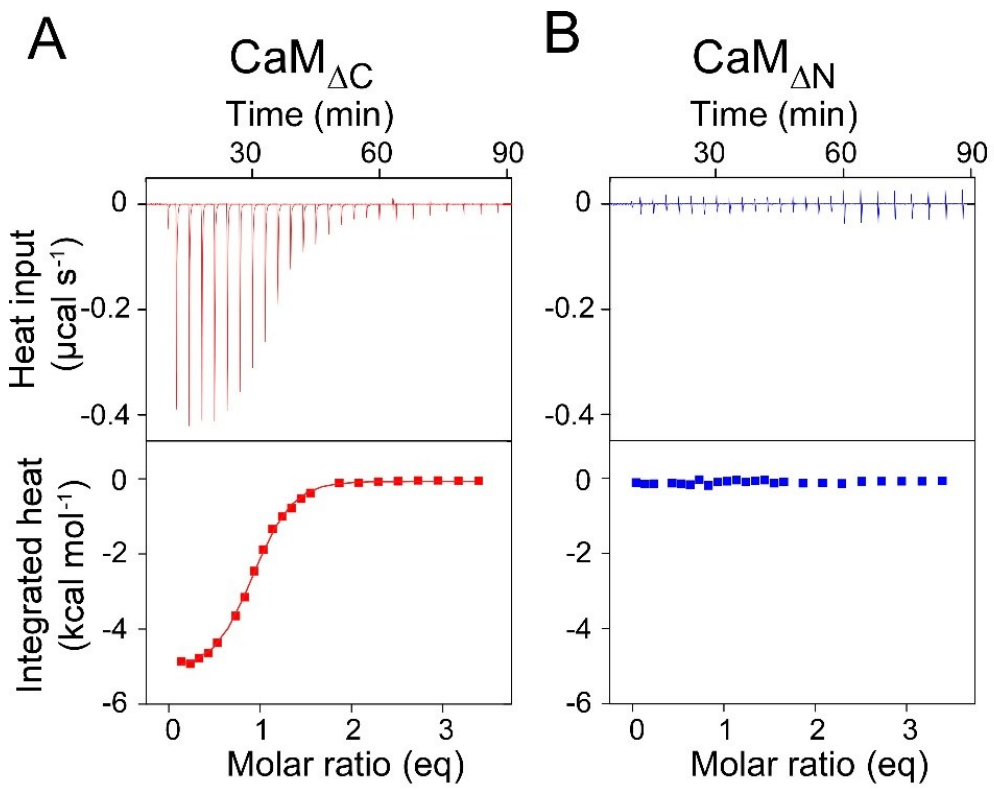

Figure S3. ITC thermograms for CBD binding of lobe-separated CaM molecules. Upper panels/raw data for sequential injections of 1 mM of CBD into 0.05 mM of CaM solutions. Lower panels represent the data points obtained by integration of the peaks in the upper thermograms, and plotted against the molar ratios. (*A*) $CaM_{\Delta C}$ and (*B*) $CaM_{\Delta N}$, in the presence of Ca^{2+}. Interestingly, despite having strong affinity between the C-lobe of CaM and CBD, this thermogram did not generate clear heat events (*B*).

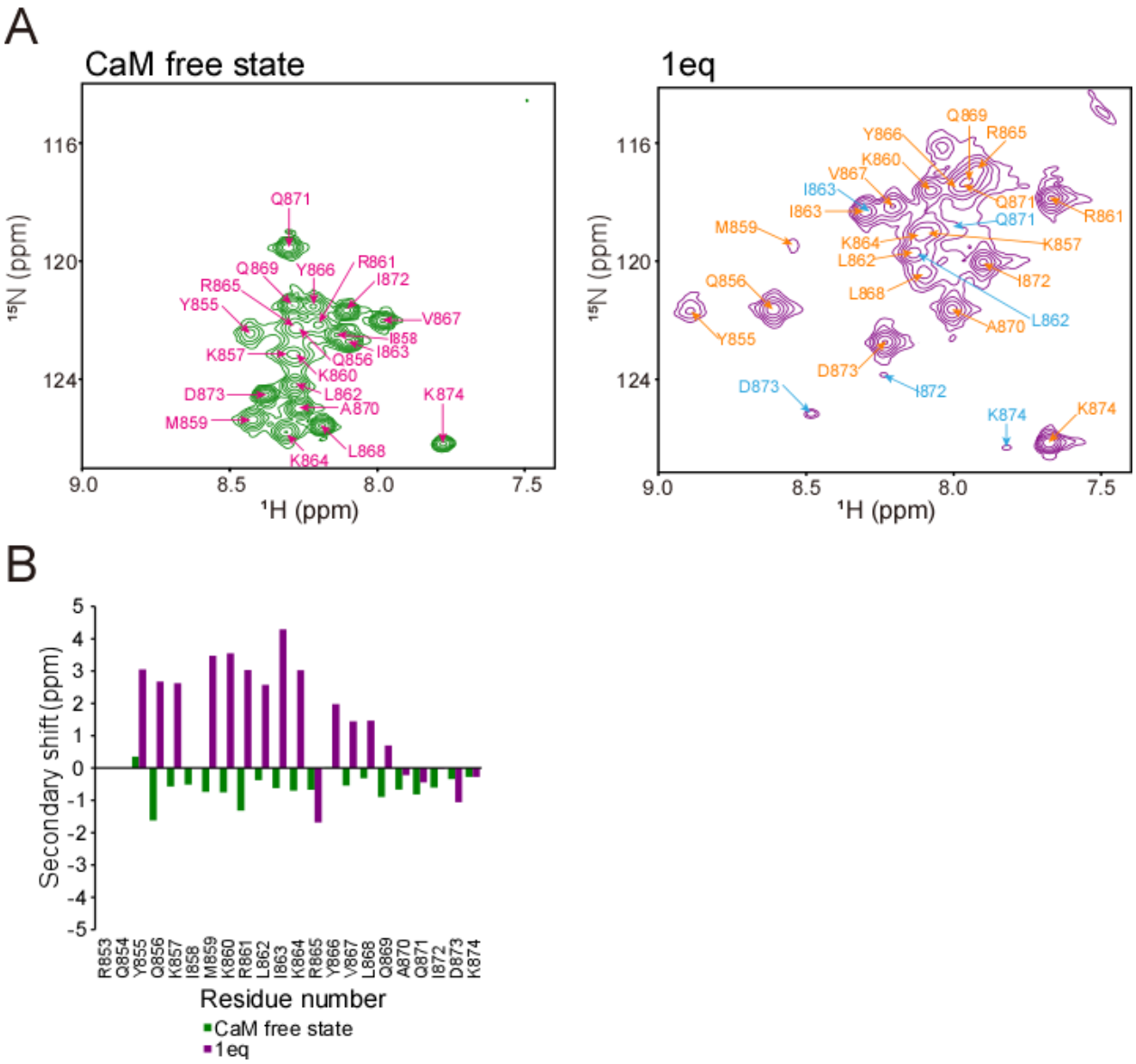

Figure S4. NMR analysis of the binding of $^{13}C,^{15}N$-CBDp to CaM. (*A*) 2D ^{1}H-^{15}N SOFAST-HMQC spectra of $^{13}C,^{15}N$-labeled CBDp in the absence (green) and the presence of 1 eq CaM (purple). In the 1 eq state, assignments are indicated for the major (orange) and minor state (cyan), which presumably correspond to the C- and N-lobe bound state, respectively. Most of the signals at the 1:2 ratio of CaM:CBDp state (in the presence of 0.5 eq of CaM, red) were extensively broadened most likely due to intermediate exchange between multiple states (free, the N- and C-lobe bound states) of $^{13}C,^{15}N$-CBDp, hence assignment was not obtained. (*B*) Plots

of the secondary chemical shifts of $^{13}C,^{15}N$-CBDp obtained in the absence (green) and the presence of 1 eq CaM (purple). The secondary shift was calculated according to the formula: [$\delta^{13}C\alpha$ (measured) - $\delta^{13}C\alpha$ (random coil reference)] - [$\delta^{13}C\beta$ (measured) - $\delta^{13}C\beta$ (random coil reference)]. Small absolute values seen for the CaM free state show that the peptide is in random coil in solution. However, from Y855 to K864, addition of 1 eq of CaM gave rise to a substantial increase in secondary shift values, indicating formation of an α-helix in this region. For the assignments of $^{13}C,^{15}N$-labeled CBDp, 3D HNCA, HNCACB, HN(CO)CA and CBCA(CO)NH spectra were recorded with or without non-labeled CaM. The chemical shift deviations from the reference values were used to assess the secondary structure propensities within the assigned residues.[4]

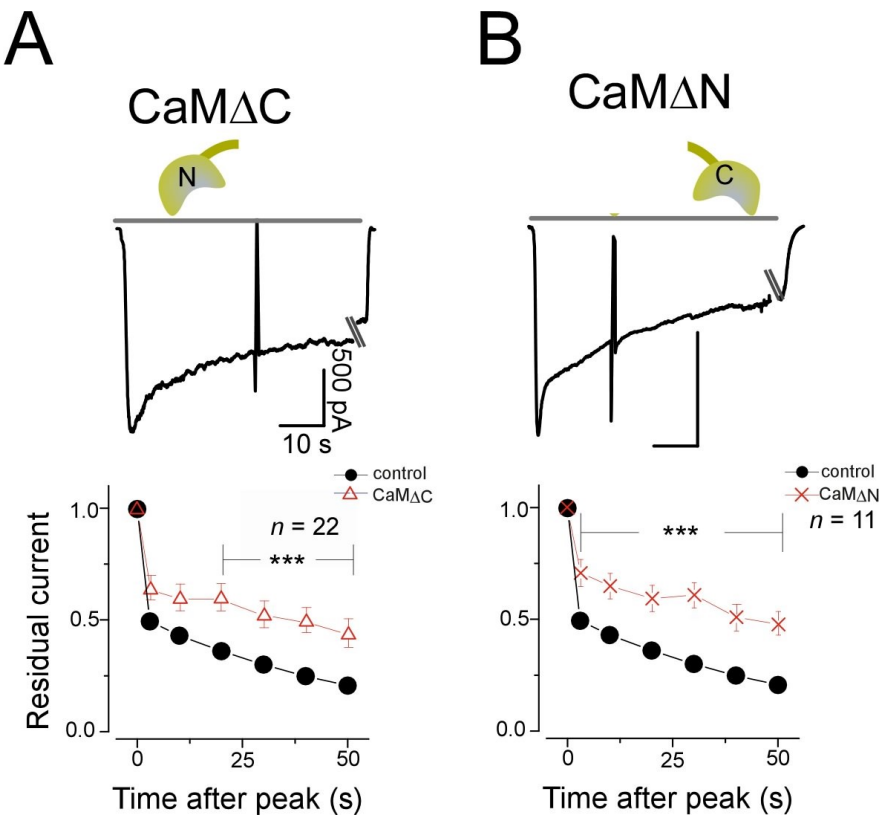

Figure S5. Effect of single-lobe CaM on CDI (*A*) CCh-induced TRPC6 current trace with N-lobe only CaM ($CaM_{\Delta C}$) recorded at [1EG/0.3Ca] (upper). Fractions of residual current, plotted as a function of time after the peak (lower). Black circles indicate data from $TRPC6_{WT}$ with M_1R and CaM_{endo} (n = 14) while open triangles represent $CaM_{\Delta C}$ with $TRPC6_{WT}$ and M_1R transfected cells (n = 22). (*B*) Representative TRPC6/M_1Rcurrent traces with C-lobe only CaM ($CaM_{\Delta N}$). The *P*-values were calculated using One-way ANOVA, ***$P < 0.001$.

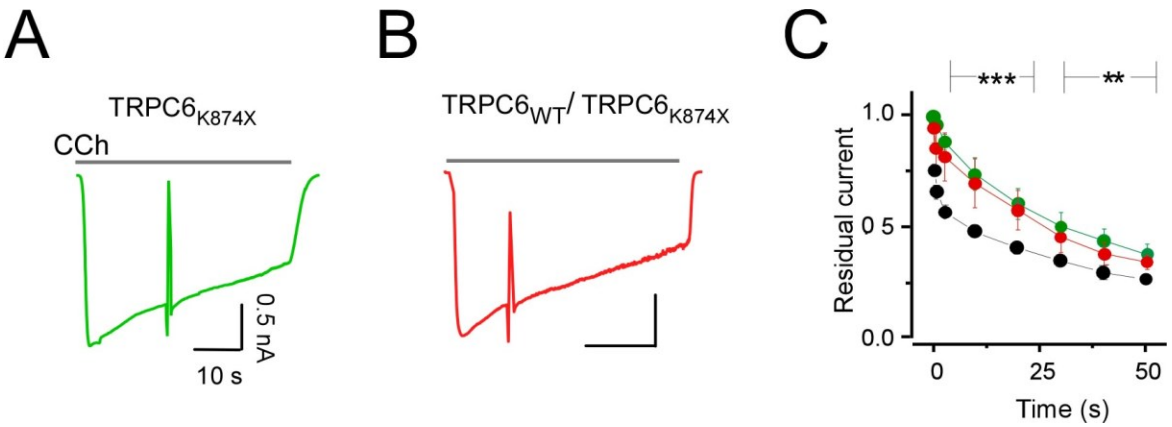

Figure S6. Current traces of (*A*) Homo ($TRPC6_{K874X}$) and (*B*) Hetero ($TRPC6_{WT}/TRPC6_{K874X}$) channels expressed in HEK293 cells. (*C*) Fractions of residual current, plotted as a function of time after the peak. Black circles indicate data from TRPC6 with M_1R transfected cells only (control), while green and red circles represent $TRPC6_{K874X}$ and $TRPC6_{WT}/TRPC6_{K874X}$ transfected cells, respectively (n = 9 and 5). The P-values were calculated using one-way ANOVA, *** and ** $P < 0.001$ and <0.01, respectively.

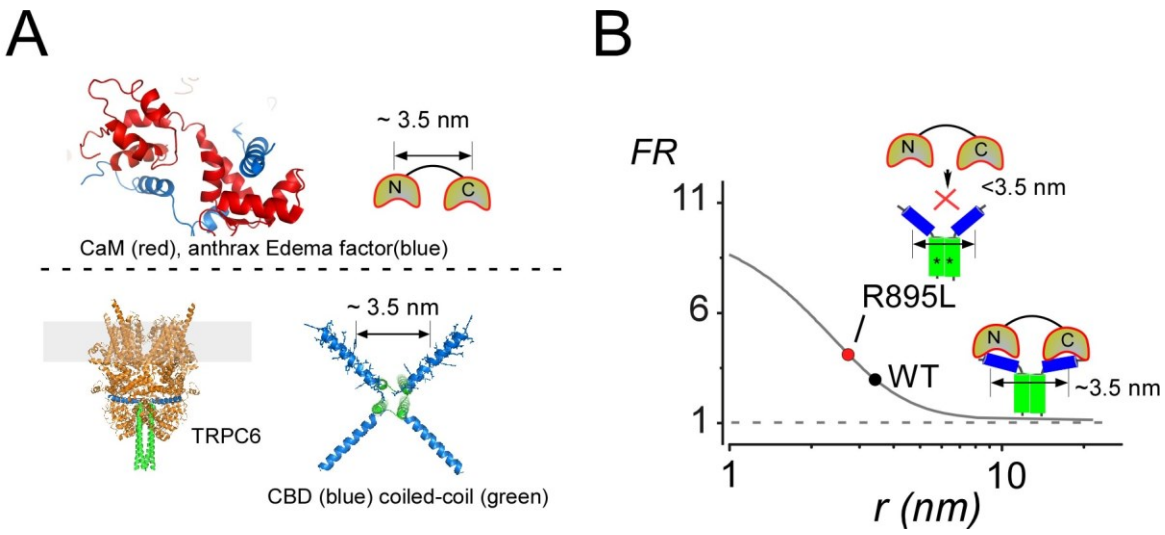

Figure S7. Effective distance between CBDs for CaM binding. (*A*) An averaged distance between N-and C-lobe of CaM is ~3.5 nm in a 1:2 complex structure (PDB, 1K90)(upper).[5] Cryo-EM structure of TRPC6 (PDB, 5YX9).[6] The distance between $TRPC6_{Y866}$ residues in the vicinal CBD is ~3.5 nm (lower). (*B*) FRET based distance estimation for CBD-CCs. FRET is a strongly distance-dependent process between a donor and an acceptor molecule, and it can be used for local distance measurements. From maximum FRET values between CBD-CCs (shown in Figure 3A and 4F), we could estimate minimal distance (r) between CBDs as follows, $r = (R_0^6/(FR_{max} - 1)/(FR_{max,E=1} - 1) - R_0^6)^{1/6} - \alpha$, where R_0 is the Förster distance (5.4 nm for CFP/YFP pair), $FR_{max,E=1}$ is the maximum FR value when FRET efficiency is 100% (we used the value of 11). α is a correction distance which contains several components such as a distance from chromophore to the surface of fluorescent protein and the linker length (we used α = ~ 3 nm).[7] Based on this equation, wild-type CBD-CCs can be calculated r = 3.2 nm which distance is close to that between CBDs in the cryo-EM structure, as mentioned above. However, the distance between $CBD\text{-}CC_{R895L}$

segments can be calculated ~0.5 nm (5 angstrom) shorter than the wild-type CBD-CC, along with the same α value. This observation suggests that CaM and CBD-CC_{R895L} complex may be in an inaccurate structure for the channel gating thereby impairing CDI.

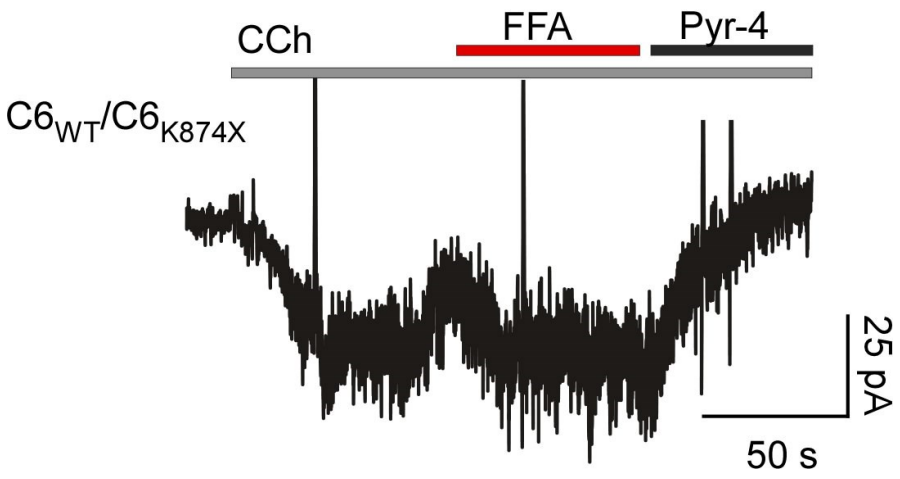

Figure S8. Potentiating agent and inhibitor effect on TRPC6-like currents in $C6_{WT}/C6_{K874X}$ channels with M_1R expressed in cultured podocytes. The cells were held at -50 mV. Whole-cell current trace exhibiting the potentiative effect of FFA (100 μM), and the inhibitory effect of Pyr-4 (10 μM).

Table S1 Binding parameters for CaM and TRPC6-CBD by FRET measurements

YFP-tag	CFP-tag	*n*	dFR_{max}	$K_{d,eff}$	K_d (μM)*
CBD_{WT}	CaM_{WT}	26	5.05	2940±580	0.78
CBD_{WT}	CaM_{12}	19	5.10	1260±53	0.03**
CBD_{WT}	CaM_{34}	12	3.23	11630±1100	4.8**
CBD_{WT}	CaM_{1234}	13	5.01	56010±2300	12640.1
CBD_{I863A}	CaM_{WT}	32	4.43	8550±2050	26.04
CBD_{R865Q}	CaM_{WT}	15	5.51	8560±310	26.12
CBD_{L868A}	CaM_{WT}	15	5.52	6170±400	8.89
CBD_{WT}	CBD_{WT}	53	2.40	8659±679	3.77
$CBDCC_{WT}$	$CBDCC_{WT}$	55	2.94	4162±794	1.52
$CBDCC_{Q889K}$	$CBDCC_{Q889K}$	53	2.96	9755±544	4.32
$CBDCC_{R895C}$	$CBDCC_{R895C}$	71	3.68	2678±824	0.78
$CBDCC_{R895L}$	$CBDCC_{R895L}$	79	4.12	1860±1789	0.37
$CBDCC_{E897K}$	$CBDCC_{E897K}$	64	3.10	9324±1158	4.10

*$K_{d,}$ is calculated based on a linear regression of known K_d values from ITC and its corresponding $K_{d,eff}$ (unitless). ** values from ITC experiments

Table S2 Thermodynamic parameters of the binding of CaM to CBD

	N	K_d **(μM)**	***ΔH*** **(kcal mol^{-1})**	**-T*ΔS*** **(kcal mol^{-1})**	***ΔG*** **(kcal mol^{-1})**
CaM_{WT} (Site 1)	0.53 ± 0.10	0.03 ± 0.01	-0.89 ± 0.53	-9.42 ± 0.21	-10.30 ± 0.39
CaM_{WT} (Site 2)	0.68 ± 0.05	4.84 ± 1.45	-4.03 ± 0.04	-3.23 ± 0.21	-7.27 ± 0.17
$CaM_{\Delta C}$*	0.91 ± 0.01	2.59 ± 0.63	-5.07 ± 0.19	-2.56 ± 0.04	-7.63 ± 0.15
$CaM_{\Delta N}$*	N/A	N/A	N/A	N/A	N/A

The parameters were obtained by fitting the ITC data to an independent two-sites or single-site (*) binding model. *N* indicates the number of binding sites. N/A- data not available. Data was obtained from three independent measurements.

Table S3 Primers for the constructions

Constructs/Vector	Forward 5'–3'	Reversal 3'–5'
hTRPC6_K874X/pIRESn	GCCCAGATAGATTAGGAGAGTGATG	CATCACTCTCCTAATCTATCTGGGC
hTRPC6_Q889K/pIRESn	GAAGGAAATTAAGAAGGACATCTCAAG	CTTGAGATGTCCTTCTTAATTTCCTTC
hTRPC6_R895C/pIRESn	CATCTCAAGTCTCTGCTATGAACTCC	GGAGTTCATAGCAGAGACTTGAGATG
hTRPC6_R895L/pIRESn	GACATCTCAAGTCTCCTCTATGAACTCC	GGAGTTCATAGAGGAGACTTGAGATGTC
hTRPC6_E897K/pIRESn	GTCTCCGCTATAAACTCCTTGAAG	CTTCAAGGAGTTTATAGCGGAGAC
CBDCC (for FRET measurement) /pIRESn	GCGGCCGCAAGACAATATCAGAAAATAATGAAAAG	CCCTCTAGATGCGGCCGCTCTATTGGTTTCCTCTT
CBD (for FRET measurement) /pIRESn	GCGGCCGCAAGACAATATCAGAAAATAATGAAAAG	CCCTCTAGATCACTTATCTATCTGGGCCTG
CBDCC (for Protein expression) /pIRESn	CGTCATATGAGACAATATCAGAAAATAATGAAAAG	GGAATCTAGAGGATCCTTATFTATCCTC
AcGFP (for GFP-TRPC6 channels) /pIRESn	GAAGCTAGCATGGTGAGCAAGGGCGCCGAG	GATGGTACCTCCACCCTTGTACAGCTCATCCAT
hTRPC6_I863A/pIRESn	TGAAAAGGCTCGCTAAAAGATATGTACTG	CAGTACATATCTTTTAGCGAGCCTTTTCA
hTRPC6_R865Q/pIRESn	GAAAAGGCTCATTAAACAATATGTACTGCAGG	CCTGCAGTACATATTGTTTAATGAGCCTTTTC
hTRPC6_L868A/pIRESn	CATTAAAAGATATGTAGCCCAGGCCCAGATAG	CTATCTGGGCCTGGGCTACATATCTTTTAATG
hTRPC6$_{\Delta CC}$ (1-875 a.a.) /pIRESn	GGTTTCCAGGAAGATGCAG	CTAGATGCGGCCGCCTCCTTATCTATCTGGGC
CaM$_{\Delta}$C (1-75 a.a.) /pCI-neo	GTCGAC ATGGCTGACCAACTGA	GGGTACCTCATTTTCTTGCCATCATTG
CaM$_{\Delta}$N (76-149 a.a.) /pCI-neo	GTCGACATGAAAGACACAGAC	TCTAGACTACTTCGCTGTCATCATTTG

References

1 Grynkiewicz G, Poenie M, Tsien RY: A new generation of Ca2+ indicators with greatly improved fluorescence properties. *J Biol Chem* 260: 3440-3450, 1985

2 Itsuki K, Imai Y, Hase H, Okamura Y, Inoue R & Mori MX: PLC-mediated PI(4,5)P_2 hydrolysis regulates activation and inactivation of TRPC6/7 channels. *J Gen Physiol* 143: 183-201, 2014

3 Imai Y, Itsuki K, Okamura Y, Inoue R & Mori MX: A self-limiting regulation of vasoconstrictor-activated TRPC3/C6/C7 channels coupled to PI(4,5)P(2)-diacylglycerol signalling. *J Physiol* 590: 1101-1119, 2012

4 Luca S, Filippov DV, van Boom JH, Oschkinat H, de Groot HJ & Baldus M: Secondary chemical shifts in immobilized peptides and proteins: a qualitative basis for structure refinement under magic angle spinning. *J Biomol NMR* 20: 325-331, 2001

5 Drum CL, Yan SZ, Bard J, Shen YQ, Lu D, Soelaiman S et al.: Structural basis for the activation of anthrax adenylyl cyclase exotoxin by calmodulin. *Nature* 415: 396-402, 2002

6 Tang Q, Guo W, Zheng L, Wu JX, Liu M, Zhou X et al.: Structure of the receptor-activated human TRPC6 and TRPC3 ion channels. *Cell Res* 28: 746-755, 2018

7 Lam AJ, St-Pierre F, Gong Y, Marshall JD, Cranfill PJ, Baird MA et al.: Improving FRET dynamic range with bright green and red fluorescent proteins. *Nat Methods* 9: 1005-1012, 2012